Centennial Records of PAHs and Black Carbon in Altay Mountain Peatlands, Xinjiang, China

Nana Luo (luonana@iga.ac.cn)
Northeast Institute of Geography and Agroecology Chinese Academy of Sciences
Kunshan Bao
South China Normal University - Shipai Campus: South China Normal University
Bolong Wen
Northeast Institute of Geography and Agroecology Chinese Academy of Sciences
Rui Yu
Northeast Institute of Geography and Agroecology Chinese Academy of Sciences
Yelebolat Tuoliuhan
Xinjiang Academy of Animal Science
Xingtu Liu
Northeast Institute of Geography and Agroecology Chinese Academy of Sciences

Research Article

Keywords: Peatland, Black carbon, PAHs, δ13 CBC, Altay Mountain

Posted Date: April 28th, 2021

DOI: https://doi.org/10.21203/rs.3.rs-330367/v1

Abstract

Black carbon (BC) and polycyclic aromatic hydrocarbons (PAHs) are often used to indicate anthropogenic impacts on natural environmental changes during the past century. In this study, a 30 cm peat core was collected from the Jiadengyu (JDY) peatland in Altay Mountain and dated by the ^{137}Cs and ^{210}Pb methods. The total organic carbon, BC and PAHs contents in JDY peat core were 17.09-47.16%, 1.14-67.14 mg g^{-1} and 260.58-950.98 ng·g^{-1}, respectively. The $\delta^{13}C_{BC}$ ranged from -31.5‰ to -27.43‰, with an average of -30.52‰. Scanning electron microscope (SEM) showed that the BC particles in the peat were lumpy or irregular in shape and retained the structure of plant fiber. The PAHs ratios, $\delta^{13}C_{BC}$ and the SEM result indicated the dominant biomass combustion source of BC in the peatland. The BC content increased from 1950 to 1980 and decreased after 1980. The change of BC and $\delta^{13}C_{BC}$ is different from the national BC emission pattern, probably reflecting the impact of local agricultural exploration and thus crop burning increase.

1. Introduction

Black carbon (BC) is produced by incomplete combustion of fossil fuels or biomass in environment and plays an important role in the carbon biogeochemical process of ecosystem (Hammes et al., 2007; Meehl et al., 2008; Ramanathan and Carmichael, 2008). Global BC was emitted by 50–270 Tg C a^{-1} as residues of vegetation fires (Kuhlbusch, 1995), and 4.4 Tg C a^{-1} from fossil fuel consumption with a liner increase trend (Bond et al., 2007). In recent years, the increased industrial and agricultural activities have significantly changed the global carbon cycle through the emission of greenhouse gases and BC particles (Hu et al., 2020; Kuhlbusch, 1995). For example, BC contents in atmosphere were high up to 2 μg C. m^{-3} in Beijing and Shanghai (China), which was nearly 2.5 times of that in Gosan (Korea) (Chen et al., 2013).

Identifying sources of BC is helpful in better understanding the proportion of the influence of regional climate change and human activities on BC fluxes (Lehndorff et al., 2015; Sun et al., 2017). The formation and morphological structure of BC is related to the type of fuel, the temperature and duration of combustion (Preston and Schmidt, 2006). Previous methods for identifying soil BC sources included potassium dichromic oxidation, 375°C thermal oxidation, Thermal-light transmission carbon analyzer (TOT) and Thermoscopic carbon analyzer (TOT/RT), ratio between BC and total organic carbon (TOC) analysis, stable carbon isotope analysis ($\delta^{13}C_{BC}$) and scanning electron microscope observation (SEM) (Gao et al., 2014b; Li et al., 2019; Neupane et al., 2020). The $\delta^{13}C_{BC}$ analysis technology has been widely used in soil BC traceability analysis (Chen et al., 2013; Qi and Wang, 2019), because terrestrial plants have different stable $\delta^{13}C$ compositions, between − 20‰ and − 32‰ (C3), and between − 10‰ and − 17‰ (C4) (Bird and Ascough, 2012; Kawashima and Haneishi, 2012) due to their different photosynthesis pathways of C3, C4 and CAM (Sage and Wedin, 1999). In addition, PAHs were usually used to identify burning sources and then indicate pyrolysis carbon sources of BC due to their co-emission from burning process (Pontevedra-Pombal et al., 2012). The diagnostic ratios of PAHs are

useful for indicating the sources of PAHs, mainly by the ratios of Flt/(Flt + Pyr), BaA/(BaA + Chr) and Ant/(Ant + Phe) (Gao et al., 2018; Yunker et al., 2002).

BC is capable of absorbing and transporting polycyclic aromatic hydrocarbons (PAHs), and thus forms a potential pollution source (Lohmann and Lammel, 2004). Recently, BC and PAHs fluxes in sediment archives (e.g. lake sediment, peat bog) were widely used for reconstructing the regional environmental pollution history and evaluating the degree of natural and anthropogenic contributions (Gao et al., 2014b; Ruppel et al., 2015; Shen et al., 2020). Altay Mountain is located in the mid-high latitudes in the Alpine region, where the peat resources are abundant due to the cold and wet climate. This region is sensitive to climate change and it is gradually affected by human activities, especially with the increasing tourism. However, the research on anthropogenic impact on the wetland environment is quite limited.

In this study, a 30 cm peat profile from the Jiadengyu (JDY) in Altay Mountain was dated by the ^{137}Cs and ^{210}Pb methods, and multi-proxies including BC, 16 priorities of PAHs and $\delta^{13}C_{BC}$ were measured. The main objectives are: 1) to characterize the history of BC and PAHs fluxes in the JDY peat core; 2) to primarily reveal the main sources of BC fluxes in the Altay mountain.

2. Materials And Methods

2.1. Site description and sampling

The JDY peatland (48°30'18.72", 87°8'27.59"; 1600 m above the sea level) is located in the Altay Mountains Kanas Nature Reserve of the northwestern Xinjiang Uygur Autonomous Region, China (Fig. 1). It is an intermontane depression with an area of about 3 km^2, and is characterized by poor drainage. It belongs to the temperate continental cold climate, with annual average temperature of -0.2℃ and annual precipitation of 1065.4 mm (Zhang et al., 2018). The mountain can intercept much of the water vapor carried by the westerlies from the North Atlantic Ocean to the uplifted areas. Water supply in the peatland mainly comes from surface runoff of glacier and snow meltwater with a subequal admixture of rainfall. Modern vegetation on the peatland is dominated by Carex and *Sphagnum* spp. The structure and composition of modern vegetation around the study area is categorized as taiga and meadow steppe, which are distributed along the 1500–2600 m in the Altay Mountains. The taiga belt is dominated by larch (*Larix* sibirica) and spruce (*Picea* obovata), and the meadow steppe belt is characterized by mixed grasses and sedges (Forestry Bureau of Altay Mountains in Xinjiang, 2003).

In August 2019, a large block was dug up in the Jiadengyu peatland (marked as JDY) and then sectioned in-site at 1- cm intervals. All samples were stored at polyethylene bags and then brought back to the laboratory for cryopreservation.

2.2. Physicochemical analysis

2.2.1 Dry bulk density, water content and ash content analyses

The peat samples were put into the aluminum box of fixed volume, dried at 105℃ over 12 h, and then weighed to obtain the water content (WC, %) and dry bulk density (DBD, $g \cdot cm^{-3}$). The dry samples were transferred into muffle furnace at 550 ℃ over 4 h for complete combustion. The ash content (Ash, %) was calculated through the loss on ignition method. These physicochemical measurements and the geochemical analyses below were conducted in the Analysis and Test Center of Northeast Institute of Geography and Agroecology, Chinese Academy of Sciences (CAS).

2.2.2 Total organic carbon

About 1 g of dry peat samples were ground to 200 mesh and were digested sufficiently by 3 mol/L of HCl to fully remove the carbonate. Then, it was washed to neutral with deionized water, and dried after centrifugation. The dry samples were ground and weighed for TOC analysis by the element analyzer (Italy Euro Vector Company, EA 3000 type).

2.2.3 ^{210}Pb and ^{137}Cs dating

Approximate 5 g dry samples of each slices were ^{210}Pb- and ^{137}Cs- dated by a low-background γ-ray spectrometer with a high pure Ge semiconductor (ORTEC Instruments Ltd., USA) at the State Key Laboratory of Lake Science and Environment, Nanjing Institute of Geography and Limnology, CAS. A detailed description of the radiometric dating techniques used for this peat and the equations calculating sedimentation rate (SR) and peat accumulation rate (PAR) has been given elsewhere (Bao et al., 2012).

2.2.4 Black carbon, $\delta^{13}C_{BC}$ and SEM- ENERGY Spectrum Analysis

About 1 g dry samples were treated for 20 h in 10 ml HCl (1 mol/L) to remove inorganic carbon. Then, the contents were centrifuged and the residue was digested for 20 h with 10 mL acid mixture (3 mol/L HCl + 22 mol/L HF, a volumetric ratio of 1:2). The samples were then centrifuged and the residue were soaked in 10 ml HCl (1 mol/L) for 10 h. The residue is regarded to consist of organic matter, kerogen and BC. The 0.1 mol/L of NaOH (30 ml, 12 h, twice) was used to remove humid acid, and removed kerogen by $K_2Cr_2O_7$ (0.1 mol/L) and H_2SO_4 (2mol/L) mixed solution (60 h, and keep mixture yellow). All steps were treated in 55℃ bath. The residual carbon as BC and $\delta^{13}C$ in residual carbon as $\delta^{13}C_{BC}$ were quantified by a continuous-flow isotope ratios mass spectrometer (CF-IRMS) which consists of an EA (Flash, 2000 series) coupled to a Finnigan MAT 253 mass spectrometer. BC reference material (charred wood) produced in the Department of Geography at the University of Zurich (Hammes et al., 2006) was used to verify the BC measurement method. The particle size, morphology and porous structure of BC were analyzed by JSM–IT 500 HR microscope (Hitachi, Tokyo, Japan), which can perfectly combine the large field optical CCD images and SEM images until the smooth operation of high magnification observation,

real-time analysis, integration of SEM and EDS. Before the observation, it is necessary to remove the carbonate and silicate in the sample (Liu et al., 2019; Zhan et al., 2016).

2.2.5 PAHs analysis

20 g peat samples combined with Na_2SO_4 (20 g) were extracted with 20 ml of hexane acetone (1:1, v/v) at 20 ℃ under ultra-sonication. The extract was then concentrated and solvent-exchanged with hexane in a rotary evaporator. The separation was performed with a Na_2SO_4-silica gel-Na_2SO_4 column under 40 mL pentane solvent leaching. PAHs were eluted with hexane dichloromethane (2:3, v/v) after aliphatic ethers had been removed with pentane. The elution solution was again concentrated, solvent-exchanged with hexane comma and blown to 1 ml. The instrumental analysis was performed with a GC/MS system (QP5050A). The SEPA Institute standard samples of 16 priority PAHs standard mixtures were adopted as external standards for quantitative analysis, and the recovery rates were around 80–110% (Cong et al., 2016).

2.3. Statistical analysis

Descriptive statistical analyses were conducted to calculate the means, ranges, and standard deviations of the peat parameters. Moreover, linear regression analysis was used to investigate the relationship between BC content in JDY peat core and TOC, PAHs, respectively. These procedures were performed using SPSS 22 software package. Statistical significance was determined at the $P = 0.05$ level.

3. Results

3.1 Physicochemical properties of peat samples

The DBD and Ash decreased while TOC and WC increased from 1–7 cm and from 11–18 cm; DBD and Ash increased while TOC and WC decreased from 7–11 cm and from 18–30 cm (Fig. 2). The DBD value varied from 0.12 to 0.29 g cm^{-3}, and the mean value was 0.18 g cm^{-3} of the whole peat core. The DBD at 18–30 cm (mean: 0.15 g cm^{-3}) were lower than those at 1–11 cm (mean: 0.21 g cm^{-3}). The Ash ranged between 11.9% and 65.31%, with an average of 37.73% of the whole peat core. In addition, Ash (mean: 27.21%) at 18–30 cm were lower than those at 1–11 cm (mean: 55.45%). The TOC of whole peat core ranged from 17.09–47%, with an average value of 33.84 % and the highest value was 37.72% at 18 cm and the lowest value (17.09%) at 11 cm. The WC ranged between 47.09% and 64.36% and the average was 58.89% of the whole peat core.

3.2 Peat chronology

The ^{210}Pb and ^{137}Cs activity decreased with depth in JDY peat profile (Fig. 3). Ages and sedimentation rates were calculated using the CRS Model by the MATLAB 2012a software. The activities of ^{210}Pb and ^{137}Cs decreased with depth downward. The peat record covered about 160 years to reach back to A.D. 1860. The mean SR was 0.47 cm y^{-1} and the PAR is 0.06 g·cm^{-2} y^{-1}.

3.3 Temporal variation of BC, $\delta^{13}C_{BC}$ and PAHs

The average BC content was 21.06 mg g^{-1}, with a range of 1.14–67.14 mg g^{-1} in the JDY peat core. The range of $\delta^{13}C_{BC}$ was from − 31.5‰ to -29.42‰ with a mean of -30.52‰. During 1860–1950, the BC and $\delta^{13}C_{BC}$ consistently showed a relative stable pattern (Fig. 4a, b). From 1950 to 1980, the BC and $\delta^{13}C_{BC}$ showed an obviously increase trend. After 1980, the BC decreased obviously with time but the $\delta^{13}C_{BC}$ did not show consistent variation with the BC. The total PAHs in JDY peat core were 260.59–950.98 ng g^{-1}, and showed similar variation trend with the BC (Fig. 4a, c). During the nearest 10 years, the PAHs showed a minor increasing trend, which was different from the BC variation.

3.4 PAHs composition

The PAHs was mainly composed of low molecular weight compounds (2–3 rings, except Nap, Any), and the content of Any, Flu and Phe content was the highest (Fig. 5). The content of Ana, Flu and Phe prior to the 1950 (n = 6) was lower than that during 1950–1980 (n = 8), and the content of Ana, Flu and Phe was the lowest after 1980 (n = 17). The concentration of high molecular weight PAHs (IcP, BaP) prior to the 1950 was higher than the periods 1950–1980 (n = 8) and after 1980 (n = 16). For middle molecular weight PAHs (BaA, Chr) no significant difference was observed among the 3 periods, whereas for the Flt and Pyr higher content during 1950–1980 was compared to those before 1950 and after 1980.

4. Discussion

4.1 Comparison of black carbon over the world

The average content of BC in the JDY peat profile was 21.06 mg g^{-1}, which was similar with the average BC content of 24.85 mg g^{-1} in Tuqiang peat in Great Hinggan Mountains, China (Cong et al., 2016). Compared to other soils (e.g. forest soil, loess) and sediments (e.g. lake sediment, coastal sediment), contents of BC in the peats were the highest (Table 1), and represented an important stable component of the global soil carbon pool.

4.2 Black carbon source

The $\delta^{13}C_{BC}$ values of C3 plant combustion are generally lower than − 27‰, and those of fossil fuel combustion range from − 23‰ to -26‰ (Bird and Ascough, 2012; Saiz et al., 2015). The $\delta^{13}C$ values in automobile exhaust gas range from − 22‰ to -25‰, and those of coal combustion range from − 24‰ to -26‰ (Glaser et al., 2005). Here the $\delta^{13}C_{BC}$ in the JDY peat core varied from − 29.42‰ to -31.5‰, with an average of -30.52‰, which is in the range of C3 plant burning type (-27‰ to -33‰). Therefore, the BC in the JDY peatland are dominantly from C3 plants burning. Because BC and PAHs were always co-emitted from the same pyrolysis sources, the proportion of different PAHs sources could also be used to estimate the proportion of BC sources (Bucheli et al., 2004; Cao et al., 2020; Yunker et al., 2002).

BaA/(BaA + Chr) > 0.35, Flt/(Flt + Pyr) > 0.5 and Ant/(Ant + Phe) < 0.1 indicate that PAHs are mainly from biomass combustion (Gao et al., 2018). In this study, the BaA/(BaA + Chr) ratio, Flt/(Flt + Pyr) ratio and Ant/(Ant + Phe) ratio were 0.45, 0.56 and 0.13 respectively (Fig. 6). Therefore, the main source of PAHs is biomass combustion in JDY profile, which is consistent with the main source revealed by the $\delta^{13}C_{BC}$ values.

Previous studies found that the BC particles emitted by diesel vehicle combustion were less than 50 nm and spherical in shape, with an agglomeration and long chain (Accardidey, 2003; Wang et al., 2015). The particle size and morphology of BC particles derived from gasoline vehicles are similar to those of diesel vehicles, but the polymerization is more obvious. BC particles emitted by coal burning are generally porous and not spherical in shape (Zhan et al., 2016). BC particles from biomass combustion releases are lumpy or irregular in shape and retain the structure of plant fibers (porous or tubular) (Masiello, 2004). The BC of samples at depths of 18 cm and 28 cm was lumpy or irregular in shape, which retained the structure of plant fibers (porous or tubular) (Fig. 7a-d), and indicated the effects of biomass combustion.

4.3 Black carbon temporal variation

Compared with the regional background of China's BC emissions (Gao et al., 2014b), this study attempts to analyze the BC emission pattern in the Altay region during the last 150 years. The concentration of BC emissions in China has been increasing, especially after 1980, which is mainly controlled by the increase of industrial emissions (Fig. 8a (Gao et al., 2014a)). However, the changes of BC content and BC flux in JDY show an increasing trend before 1980 but a decreasing trend after 1980 (Fig. 8b). This is because the BC in JDY peat profile is mainly from biomass combustion, as discussed above. It was reported that the cultivated land area in 1949 from 9.43 km^2 increased to 115.29 km^2 in 1980 in Altay area (Statistics, 2018). As a result, BC content in the JDY peatland significantly increased from 1950 to 1980. The decrease in the BC record in the peat is probably a response to the increasing regional environmental protection.

5. Conclusion

The average accumulation rate of BC in JDY peatland was 0.47g·cm^{-2} yr^{-1} since the 1860s. The range of $\delta^{13}C_{BC}$ was from − 31.5‰ to -29.42‰. The $\delta^{13}C_{BC}$, the PAHs composition ratios and the SEM results indicated the BC source was dominated by burning C3 plants. The historical variations in BC content and flux was different from the national BC emission pattern in China. The JDY peat recorded an increase of BC emission in 1950–1980 probably due to the agricultural exploration and thus increasing crop burning. The decrease in the peat BC record after 1980 would be related to the increasing environmental protection.

Declarations

Acknowledgments

The authors gratefully acknowledge the assistance of the Analysis and Test Center of the Northeast Institute of Geography and Agroecology, CAS. Part of the work is related with Nana Luo Ph.D. thesis.

Funding

This research was funded by the National Basic Research Program of China (no. 2013FY111800), National Nature Science Foundation of China (no. 41971113), the Science and Technology Development Program of Jilin Province (Support Xinjiang), National Natural Science Foundation of China (no. 41701372) and Natural Science Foundation of Jilin Province (no. 20190103161JH).

Author contributions

All authors contributed to the design and development of this manuscript. Nana Luo and Kunshan Bao carried out the data analysis and prepared the first draft of the manuscript; Xingtu Liu and Bolong Wen is the advisor of Nana Luo and contributed many ideas to the study; Rui Yu and Yelebolat • Tuoliuhan provided experimental data and advice on the structuring of the manuscript. All authors read and approved the final manuscript.

Compliance with ethical standards

Conflict of interest No conflict of interest exits in the submission of this manuscript, and manuscript is approved by all authors for publication

Ethics approval and consent to participate Not applicable for this **s**ection.

Consent for publication Not applicable for this section

Availability of data and materials Not applicable for this section

References

1. Accardidey AM (2003) Black carbon in marine sediments: quantification and implications for the sorption of polycyclic aromatic hydrocarbons. Massachusetts Institute of Technology 20:171–177
2. Bao K, Xing W, Yu X, Zhao H, McLaughlin N, Lu X, Wang G (2012) Recent atmospheric dust deposition in an ombrotrophic peat bog in Great Hinggan Mountain, Northeast China. Sci Total Environ 431:33–45
3. Bird MI, Ascough PL. Isotopes in pyrogenic carbon: A review. Organic Geochemistry 2012; 42: 1529-153910.1016/j.orggeochem.2010.09.005
4. Bond TC, Bhardwaj E, Dong R, Jogani R, Jung S, Roden C et al. Historical emissions of black and organic carbon aerosol from energy-related combustion, 1850–2000. Global Biogeochemical Cycles

2007; 2110.1029/2006gb002840

5. Bucheli TD, Blum F, Desaules A, Gustafsson O. Polycyclic aromatic hydrocarbons, black carbon, and molecular markers in soils of Switzerland. Chemosphere 2004; 56: 1061-107610.1016/j.chemosphere.2004.06.002
6. Cao W, Geng SY, Zou J, Wang YY, Guo YQ, Zhu Y et al. Post relocation of industrial sites for decades: Ascertain sources and human risk assessment of soil polycyclic aromatic hydrocarbons. Ecotoxicology and Environmental Safety 2020; 198: 910.1016/j.ecoenv.2020.110646
7. Chen B, Andersson A, Lee M, Kirillova EN, Xiao QF, Krusa M et al. Source Forensics of Black Carbon Aerosols from China. Environmental Science & Technology 2013; 47: 9102-910810.1021/es401599r
8. Cong JX, Gao CY, Zhang Y, Zhang SQ, He JB, Wang GP. Dating the period when intensive anthropogenic activity began to influence the Sanjiang Plain, Northeast China. Scientific Reports 2016; 6: 910.1038/srep22153
9. Cong Z, Kang S, Gao S, Zhang Y, Li Q, Kawamura K. Historical Trends of Atmospheric Black Carbon on Tibetan Plateau As Reconstructed from a 150-Year Lake Sediment Record. Environmental Science & Technology 2013; 47: 2579-258610.1021/es3048202
10. Cordeiro RC, Turcq B, Ribeiro MG, Lacerda LD, Capitaneo J, da Silva AO et al (2002) Forest fire indicators and mercury deposition in an intense land use change region in the Brazilian Amazon (Alta Floresta, MT). Sci Total Environ 293:247 -25610.1016/s0048-9697(02)00045 – 1.
11. Gao C, Liu, Hanxiang, Cong J et al. Historical sources of black carbon identified by PAHs and delta C-13 in Sanjiang Plain of Northeastern China. Atmospheric Environment 2018
12. Gao CY, Lin QX, Zhang SQ, He JB, Lu XG, Wang GP. Historical trends of atmospheric black carbon on Sanjiang Plain as reconstructed from a 150-year peat record. Scientific Reports 2014b; 4: 710.1038/srep05723
13. Glaser B, Dreyer A, Bock M, Fiedler S, Mehring M, Heitmann T. Source apportionment of organic pollutants of a highway-traffic-influenced urban area in Bayreuth (Germany) using biomarker and stable carbon isotope signatures. Environmental Science & Technology 2005; 39: 3911-391710.1021/es050002p
14. Gustafsson O, Gschwend PM. The flux of black carbon to surface sediments on the New England continental shelf. Geochimica Et Cosmochimica Acta 1998; 62: 465-47210.1016/s0016-7037(97)00370-0
15. Hammes K, Schmidt MWI, Smernik RJ, Currie LA, Ball WP, Nguyen TH et al. Comparison of quantification methods to measure fire-derived (black/elemental) carbon in soils and sediments using reference materials from soil, water, sediment and the atmosphere. Global Biogeochemical Cycles 2007; 21: 1810.1029/2006gb002914
16. Hammes K, Smernik RJ, Skjemstad JO, Herzog A, Vogt UF, Schmidt MWI. Synthesis and characterisation of laboratory-charred grass straw (Oryza saliva) and chestnut wood (Castanea sativa) as reference materials for black carbon quantification. Organic Geochemistry 2006; 37: 1629-163310.1016/j.orggeochem.2006.07.003

17. Han Y, Cao J, Jin Z, Liu S, An Z (2010) Comparison of char and soot variations in sediments from Daihai and Taihu Lakes. Quaternary Sciences 30:550–558
18. Hu K, Zhao DL, Liu DT, Ding S, Tian P, Yu CJ et al. Estimating radiative impacts of black carbon associated with mixing state in the lower atmosphere over the northern North China Plain. Chemosphere 2020; 252: 1310.1016/j.chemosphere.2020.126455
19. Kawashima H, Haneishi Y (2012) Effects of combustion emissions from the Eurasian continent in winter on seasonal δ~(13)C of elemental carbon in aerosols in Japan. Atmos Environ 46:568–579
20. Kuhlbusch TAJ. Method for determining black carbon in residues of vegetation fires. Environmental Science & Technology 1995; 29: 2695-270210.1021/es00010a034
21. Lehndorff E, Brodowski S, Schmidt L, Haumaier L, Grootes PM, Rethemeyer J et al. Industrial carbon input to arable soil since 1958. Organic Geochemistry 2015; 80: 46-5210.1016/j.orggeochem.2015.01.003
22. Li R, Han Y, Wang L, Shang Y, Chen YJ. Differences in oxidative potential of black carbon from three combustion emission sources in China. Journal of Environmental Management 2019; 240: 57-6510.1016/j.jenvman.2019.03.070
23. Liu H, Meng Z-H, Lv Z-F, Wang X-T, Deng F-Y, Liu Y et al. Emissions and health impacts from global shipping embodied in US-China bilateral trade. Nature Sustainability 2019; 2: 1027-103310.1038/s41893-019-0414-z
24. Lohmann R, Lammel G (2004) Adsorptive and Absorptive Contributions to the Gas-Particle Partitioning of Polycyclic Aromatic Hydrocarbons:? State of Knowledge and Recommended Parametrization for Modeling. Environmental Science Technology 38:3793–3803
25. Masiello CA (2004) New Directions in Black Carbon Organic Geochemistry. Mar Chem 92:201–213
26. Meehl GA, Arblaster JM, Collins WD. Effects of black carbon aerosols on the Indian monsoon. Journal of Climate 2008; 21: 2869-288210.1175/2007jcli1777.1
27. Neupane B, Wang J, Kang S, Zhang Y, Chen P, Rai M et al. Black carbon and mercury in the surface sediments of Selin Co, central Tibetan Plateau: Covariation with total carbon. Science of the Total Environment 2020; 72110.1016/j.scitotenv.2020.137752
28. Pontevedra-Pombal X, Rey-Salgueiro L, Garcia-Falcon MS, Martinez-Carballo E, Simal-Gandara J, Martinez-Cortizas A. Pre-industrial accumulation of anthropogenic polycyclic aromatic hydrocarbons found in a blanket bog of the Iberian Peninsula. Environmental Research 2012; 116: 36-4310.1016/j.envres.2012.04.015
29. Preston CM, Schmidt MWI. Black (pyrogenic) carbon: a synthesis of current knowledge and uncertainties with special consideration of boreal regions. Biogeosciences 2006; 3: 397-42010.5194/bg-3-397-2006
30. Qi L, Wang SX. Fossil fuel combustion and biomass burning sources of global black carbon from GEOS-Chem simulation and carbon isotope measurements. Atmospheric Chemistry and Physics 2019; 19: 11545-1155710.5194/acp-19-11545-2019

31. Ramanathan V, Carmichael G. Global and regional climate changes due to black carbon. Nature Geoscience 2008; 1: 221-22710.1038/ngeo156
32. Ruppel MM, Gustafsson O, Rose NL, Pesonen A, Yang HD, Weckstrom J et al. Spatial and Temporal Patterns in Black Carbon Deposition to Dated Fennoscandian Arctic Lake Sediments from 1830 to 2010. Environmental Science & Technology 2015; 49: 13954-1396310.1021/acs.est.5b01779
33. Sage RF, Wedin DA. The Biogeography of C4 Photosynthesis: Patterns and Controlling Factors, 1999
34. Saiz G, Wynn JG, Wurster CM, Goodrick I, Nelson PN, Bird MI. Pyrogenic carbon from tropical savanna burning: production and stable isotope composition. Biogeosciences 2015; 12: 1849-186310.5194/bg-12-1849-2015
35. Shen X, Wang P, Zhang X, Cao X, Shi Y, Li X et al. Real-time measurements of black carbon and other pollutant emissions from residential biofuel stoves in rural China. The Science of the total environment 2020; 727: 13864910.1016/j.scitotenv.2020.138649
36. Smith DM, Griffin JJ, Golderg ED. Elemental Carbon in Marine Sediments: a Baseline for Burning. Nature 1973
37. Statistics XUARBo. Xinjiang Statistical Yearbook. 2018
38. Sun WW, Zhang EL, Liu EF, Ji M, Chen R, Zhao C et al. Oscillations in the Indian summer monsoon during the Holocene inferred from a stable isotope record from pyrogenic carbon from Lake Chenghai, southwest China. Journal of Asian Earth Sciences 2017; 134: 29-3610.1016/j.jseaes.2016.11.002
39. Wang HL, Nie L, Liu D, Gao MP, Wang MY, Hao ZP. Physico-chemical characterization and source tracking of black carbon at a suburban site in Beijing. Journal of Environmental Sciences 2015; 33: 188-19410.1016/j.jes.2015.05.001
40. Wang X, Peng PA, Ding ZL. Black carbon records in Chinese Loess Plateau over the last two glacial cycles and implications for paleofires. Palaeogeography Palaeoclimatology Palaeoecology 2005; 223: 9-1910.1016/j.palaeo.2005.03.023
41. Yunker MB, Macdonald RW, Vingarzan R, Mitchell RH, Goyette D, Sylvestre S. PAHs in the Fraser River basin: a critical appraisal of PAH ratios as indicators of PAH source and composition. Organic Geochemistry 2002; 33: 489-51510.1016/s0146-6380(02)00002–5
42. Zhan C, Wan D, Zhang J, Han Y, Cao J, Liu X (2016) Source Apportionment of Black Carbon in the Environment: A Review of Methods. Ecology Environmental Sciences 25:1575–1583
43. Zhang Y, Ma X, Liu X, Tong C, Yang P (2018) Preliminary study on the morphology, development process and peat accumulation rate of palsas during the holocene in the altai mountains, northern xinjiang autonomous region, northwest china. Quaternary Sciences 38:1221–1232

Tables

Tab. 1 The black carbon contents (mg g^{-1}) for different deposition archives

Types	Region	Contents (mg g^{-1})	Reference
Peatland	Altay Mountain, China	1.14-67.13	This study
Peatland	Sanjiang Plain, China	3.2-61.2	(Gao et al., 2014b)
Forest soil	Amazon, Brazilian	1-27	(Cordeiro et al., 2002)
Loess	Loess Plateau, China	1-5	(Wang et al., 2005)
Lake sediments (near urban)	Taihu, China	0.43-1.95	(Han et al., 2010)
Lake sediments	Tibetan Plateau, China	0.49-1.09	(Cong et al., 2013)
Continentals shell (near urban)	Palos Verdes Shelf, American	1.2	(Gustafsson and Gschwend, 1998)
Continentals shell	Gulf of Marine, England	0.3-1.7	(Gustafsson and Gschwend, 1998)
Pelagic sediments	Global	0.02-1	(Smith et al., 1973)

Figures

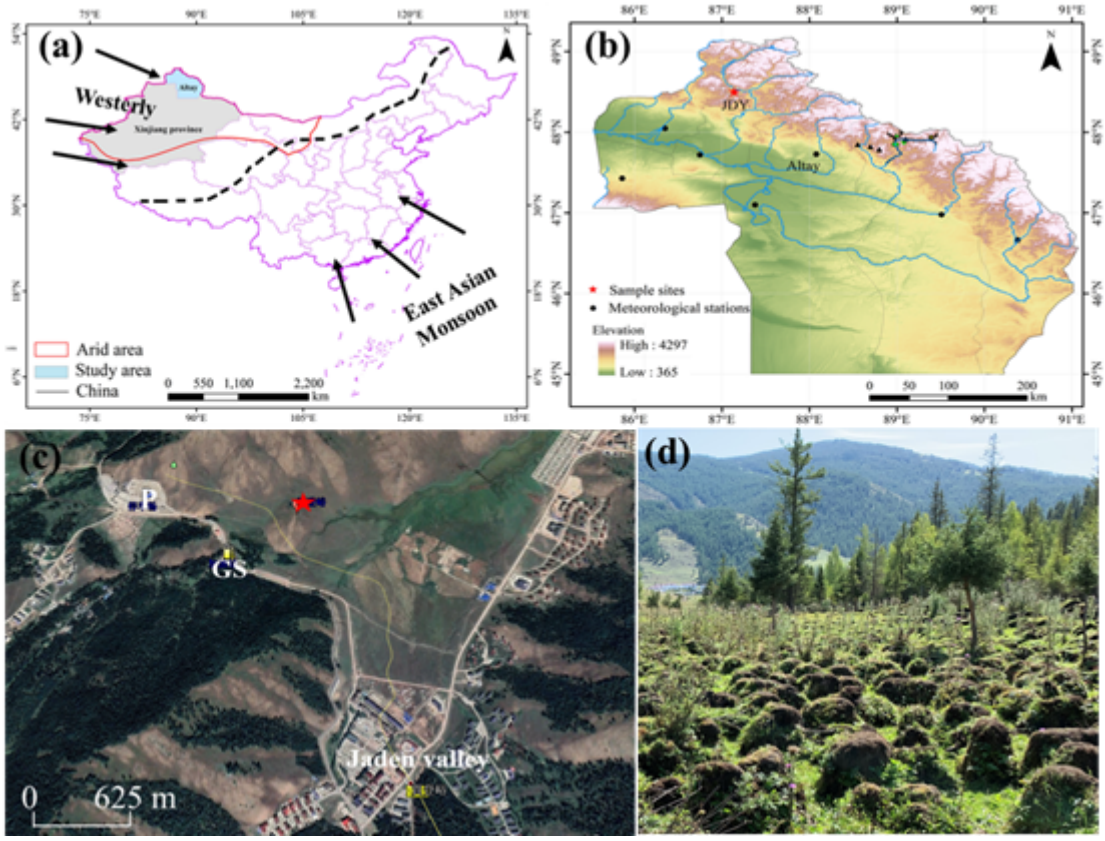

Figure 1

(a) China map showing the location of Jiadengyu in northwest China and the Asian Monsoon and the Westerly; (b) Satellite image of the Jiadengyu valley (source: Google Earth) showing the location of JDY peatland (Red five pointed star) and of a car park and gas station; (c) Geographical map showing the sampling site in Altay Mountains, northwest China; (d) Photo showing the summer scene in the studied peatland (photo in August 2019). Please refer to the Online version for the color figure. Note: The designations employed and the presentation of the material on this map do not imply the expression of any opinion whatsoever on the part of Research Square concerning the legal status of any country, territory, city or area or of its authorities, or concerning the delimitation of its frontiers or boundaries. This map has been provided by the authors.

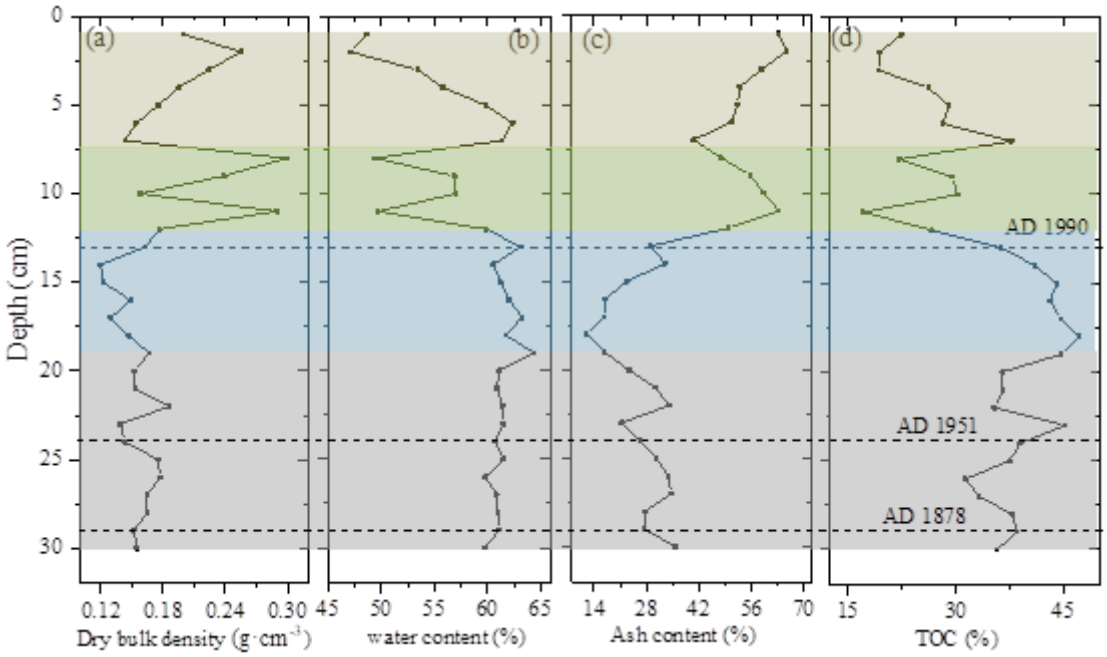

Figure 2

The depth profiles of dry bulk density (a), water content (b), ash content (c) and TOC (d) in the JDY peat core in Altay Mountains, NW China.

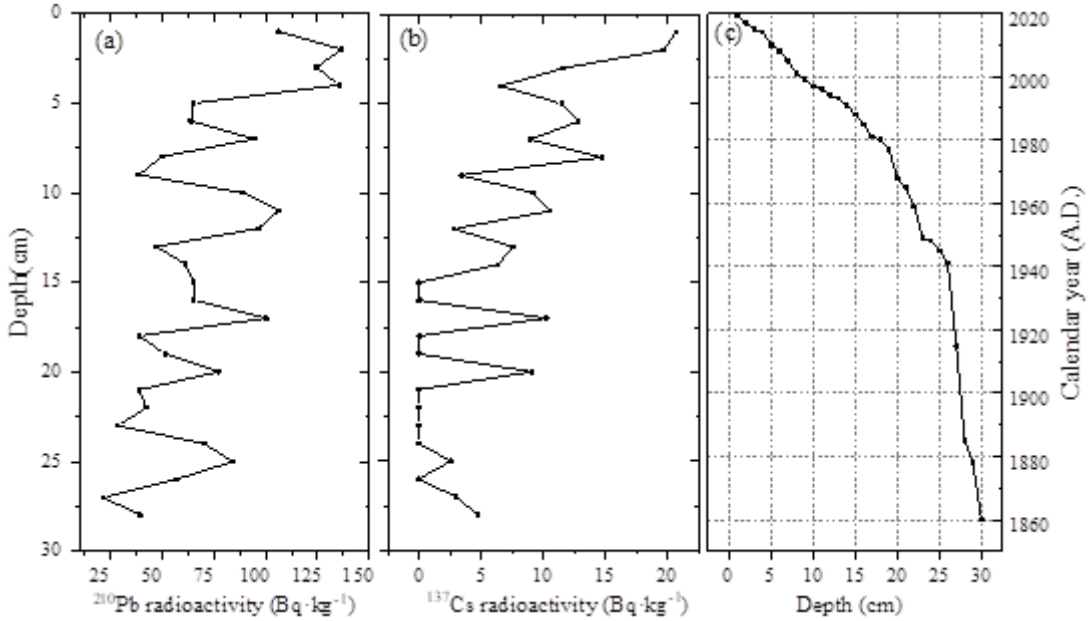

Figure 3

Radioactivity results for 210Pb (a) and 137Cs (b) activity and the CRS calculated age (c) of the JDY peat core in Altay Mountains, NW China.

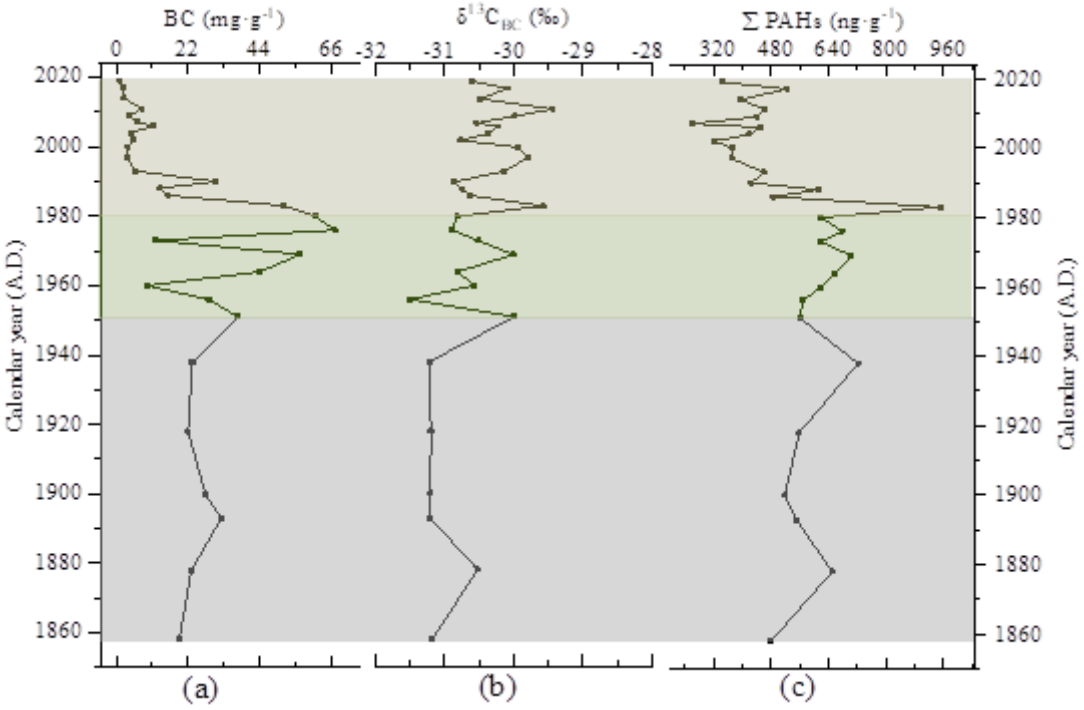

Figure 4

The contents of BC (a), δ13CBC (b) ratios and the total PAHs content (c) in the core of JDY.

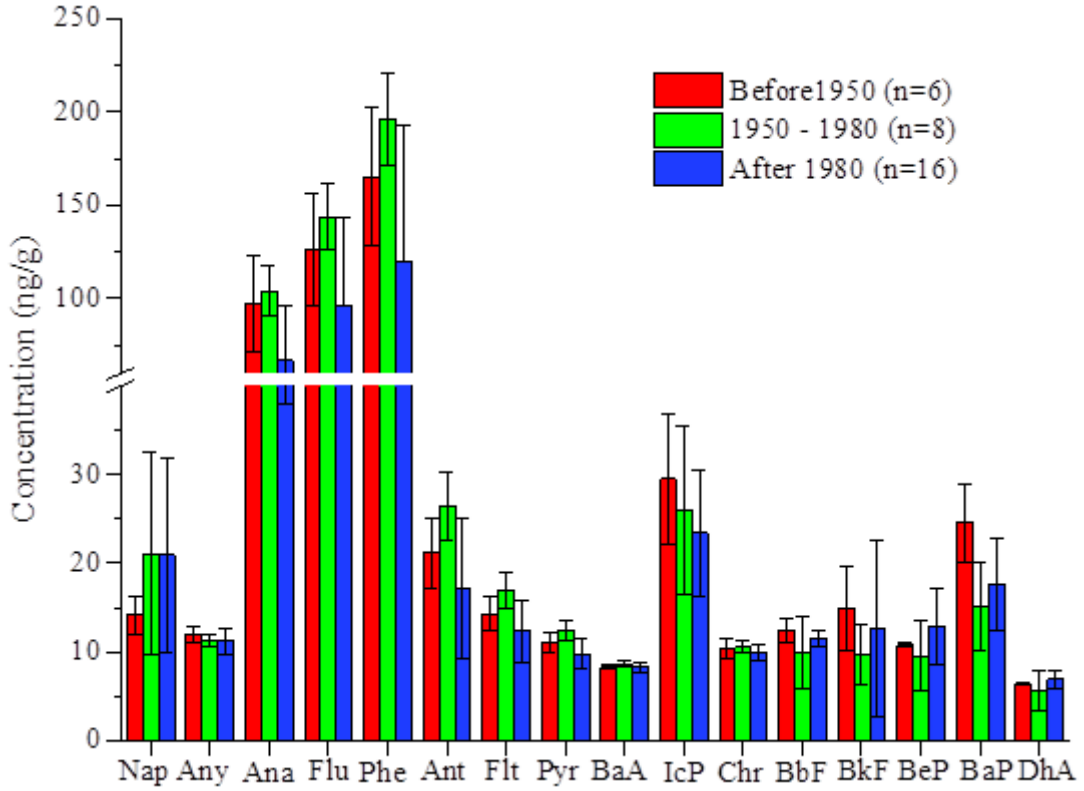

Figure 5

Profiles of PAHs in sediments from the JDY peat core, grouped according to the 3 periods. Abbreviations and full names of PAHs: Nap, Naphthalene; Any, Acenaphthylene; Ana, Acenaphthene; Flu, Fluorene; Phe,

Phenanthrene; Ant, Anthracene; Flt, Fluoranthene; Pyr, Pyrene; Chr, Chrysene; BaA, Benzo(a) anthracene; BbF, Benzo(b)fluoranthene; BkF, Benzo(k)fluoranthene; BeP, Benzo(e)pyrene; BaP, Benzo(a)pyrene; DhA, Dibenz[a,h] anthracene; IcP, Ideno(1,2,3-cd) pyrene.

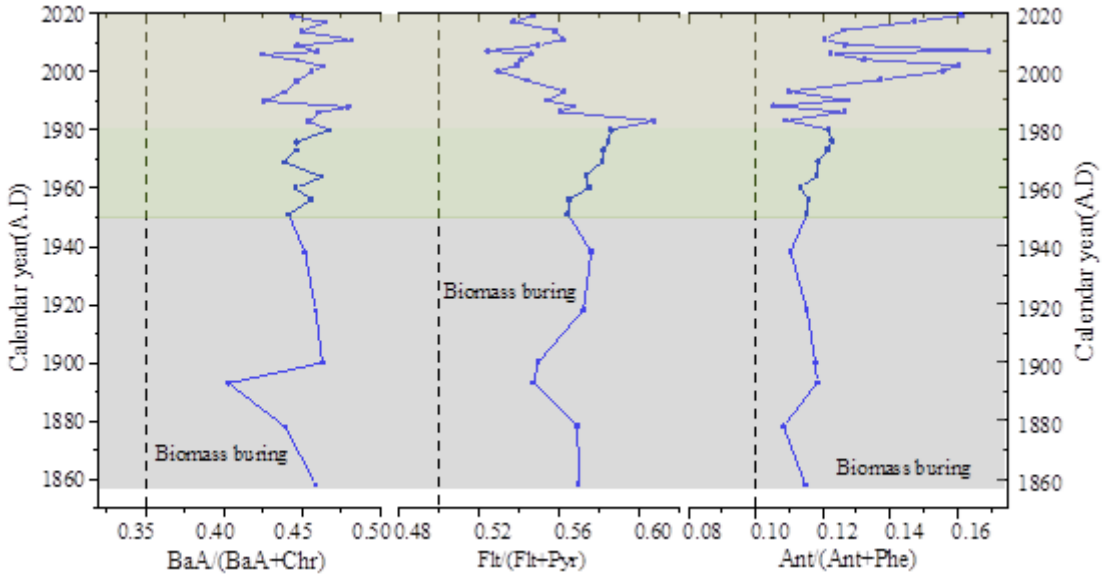

Figure 6

Variation of ratios of BaA/(BaA+Chr), Flt/(Flt+Pyr), and Ant/(Ant+Phe) in JDY peat core. The dashed lines indicated the boundaries for source assignments of PAHs were based on (Yunker et al., 2002).

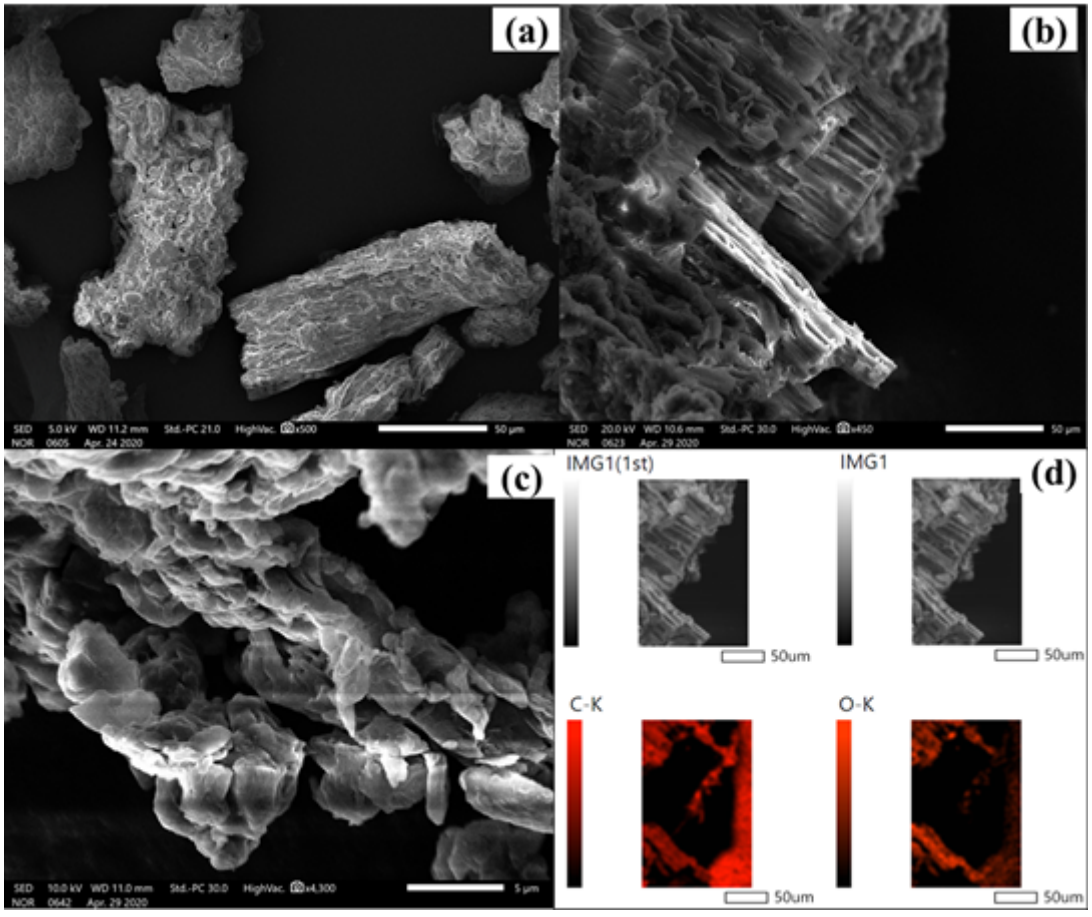

Figure 7

SEM images of BC examples from different samples. All scale bars represent 50 μm. a) Panels represent BC from biomass burning particles (BBP), b) represents Wood burning, b) represents coal combustion particles (CCP),d) represents a Major element composition.

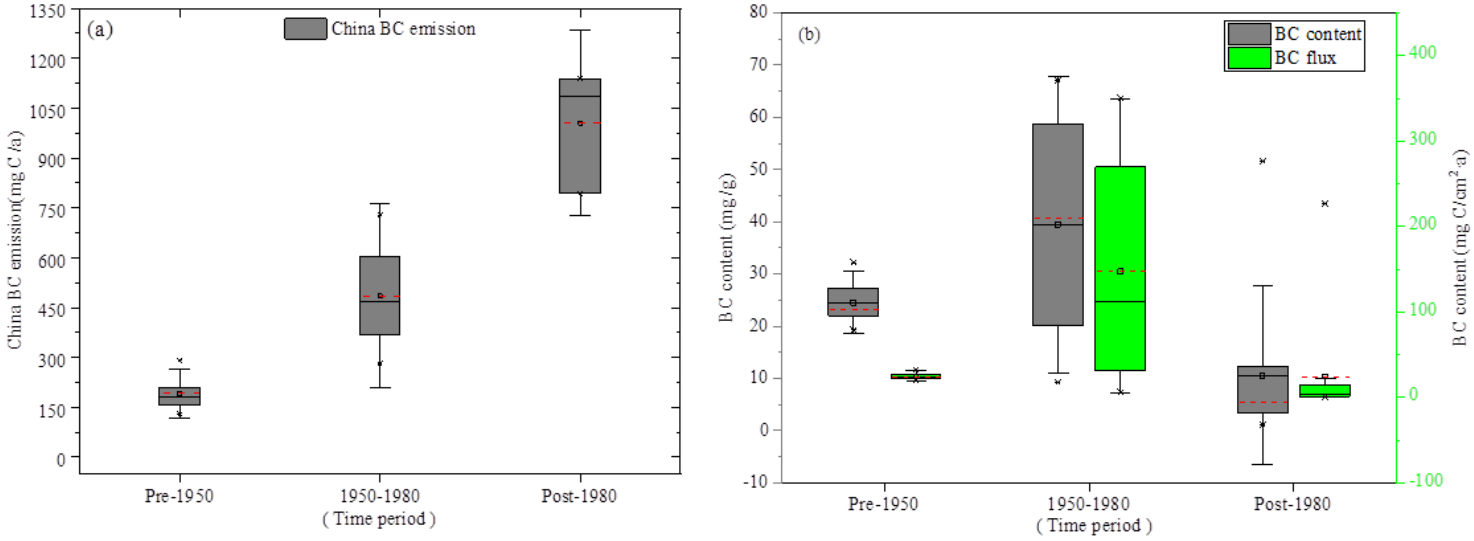

Figure 8

a) Variation of China BC emission from different period, b) BC content and BC flux from 1860 to 2019 in JDY peat core.